barrier FET's for microwave frequencies," *IEEE Trans. Electron Devices,* vol. ED-22, pp. 897–904, Oct. 1975.
[6] T. Furutsuka, M. Ogawa, and N. Kawamura, "GaAs dual gate MESFET's," *IEEE Trans. Electron Devices,* vol. ED-25, pp. 580–586, June 1978.
[7] J. L. Vorhaus, W. Fabian, P. B. Ng, and Y. Tajima, "Dual gate GaAs FET switches," *IEEE Trans. Electron Devices,* vol. ED-28, no. 2, pp. 204–211, 1981.
[8] C. Tsironis, R. Meierer, "DC characteristics aid dual-gate FET analysis," *Microwaves,* pp. 71–73, July 1981.
[9] A. S. Chu and P. T. Chen, "An osciplier up to *K*-band using dual-gate GaAs MESFET," in *MTT-S Symp. Proc.,* (Washington), 1980, pp. 383–386.
[10] J. S. Joshi and R. S. Pengelly, "Ultra low chirp GaAs dual gate FET microwave oscillators," in *MTT-S Symp. Proc.,* (Washington) 1980, pp. 379–382.
[11] C. Tsironis, P. Harrop, M. Bostelmann, "Active phase shifters at *X*-band using GaAs MESFET's," in *Proc. ISSCC* (New York), pp. 140–141, 1981.
[12] C. Liechti, E. Gowen, and J. Cohen, "GaAs microwave Schottky-Gate FET," in *Proc. ISSCC'1972,* pp. 158–159.
[13] G. Vendelin and M. Omori, "Circuit model for the GaAs MESFET valid to 12 GHz," *Electron. Lett.,* vol. 11, pp. 60–61, 1975.
[14] P. Wolf, "Microwave properties of Schottky-barrier field effect transistors," *IBM J. Res. Develop.*, vol. 14, pp. 125–141, 1970.
[15] R. H. Dawson, "Equivalent circuit of the Schottky-barrier field-effect transistor at microwave frequencies," *IEEE Trans. Microwave Theory Tech.,* vol. MTT-23, pp. 499–501, 1975.
[16] R. Pucel, H. Haus, and H. Statz, "Signal and noise properties of Gallium Arsenide microwave field-effect transistors," in *Advances in Electronics and Electron Physics*, vol. 38, New York: Academic Press, 1975, pp. 195–265.
[17] J. F. Cooper and M. S. Gupta, "Microwave characterization of GaAs MESFET and the verification of device model," *IEEE J. Solid-State Circuits,* vol. SC-12 pp. 325–329, 1977.
[18] O. Kurita and U. Morita, "Microwave MESFET mixer," *IEEE Trans. Microwave Theory Tech.,* vol. MTT-24, pp. 361–366, 1976.
[19] C. Tsironis, "Untersuchungen zum Rauschverhalten des GaAs MESFET in GHz-Bereich," Ph.D dissertation, Technical University, Aachen, 1977.
[20] A. Rabier, M. Parisot, "CAD of an octave band power FET amplifier," in *Proc. Int. Symp. SPACECAD*, (Bologna), 1979, pp. 405–406

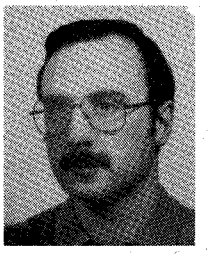

Christos Tsironis (M'81) was born in Athens in 1948. He received the Dipl. Ing. degree in electrical engineering from the University of Karlsruhe, Germany, in 1972 and the Dr. Ing. Degree from the Technical University of Aachen, Germany, in 1977.

From 1973 until 1980 he has been with the Institute of Semiconductor Electronics Technical University, Aachen, working on *X*-band diode mixers, noise, small signal, breakdown behavior, and equivalent circuit simulation of GaAs FET's and short channel Si-MOSFET's. In 1980, he joined L.E.P. (Philips Research Laboratories in France) near Paris where he is involved with work on stable FET oscillators, 12 GHz TV receiver concepts as well as characterization of dual gate FET's and applications on oscillators and self-oscillating mixers.

Roman Meierer was born in Kesten, W. Germany, in 1956. From October 1975 he has been a student of electrical engineering at the Technical University of Aachen, W. Germany. From October 1980 to January 1981, he completed an industrial training period at the Laboratoires d'Electronique et de Physique Appliquée in Paris, working on dual gate FET modeling.

Numerical Analysis of Nonlinear Solid-State Device Excitation in Microwave Circuits

ROSS G. HICKS, STUDENT MEMBER, IEEE, AND PETER J. KHAN, SENIOR MEMBER, IEEE

Abstract — **This paper presents an efficient technique for the numerical determination of voltage and current waveforms when a microwave circuit containing one or more nonlinear elements is excited by a single frequency source. The approach described here is readily applied to microwave networks represented by a large number of equivalent circuit elements, either lumped or distributed. A significant feature of this paper is the detailed investigation of the problem of convergence, using this new technique. The generality of the technique is illustrated through its application to studies of the excitation of varactor, Schottky-barrier, and IMPATT diodes in waveguide circuits. In addition, the relationship of this method to the multiple reflection approach is discussed and the convergence mechanism of this reflection technique is studied.**

Manuscript received December 11, 1980; revised October 30, 1981. This work was supported by United States ARO Grant DAA G29-76-G-0079, and by the Australian Research Grants Committee under Grant F76/15147.

The authors are with the Electrical Engineering Department, University of Queensland, St. Lucia, Queensland, 4067, Australia.

I. INTRODUCTION

THIS PAPER reports a general method for the analysis of microwave circuits which contain a sinusoidal source and one or more nonlinear devices. It is applicable to the

0018-9480/82/0300-0251$00.75 ©1982 IEEE

study of a wide range of microwave circuits including mixers, parametric amplifiers, and harmonic generators. A special feature of the approach presented here is its detailed consideration of the problem of convergence in the iterative solution process, and its provision for modification of the general procedure to facilitate convergence with any specified circuit.

The analysis of this class of microwave circuit has relied, in the main, upon the short-circuit or open-circuit assumptions, pertaining to the impedance of the circuit, at harmonics of the excitation frequency, viewed from the (single) nonlinear element terminals. Such an assumption greatly simplified the analysis, since it leads to sinusoidal voltage or current flowing through the nonlinear element. Unfortunately, this assumption can rarely be justified in a practical microwave circuit, due to the periodicity of distributed-element impedances as well as to multimode propagation at harmonic frequencies. Thus in the general case, *both* voltage and current through the nonlinear element are nonsinusoidal, when the circuit is excited by a sinusoidal source.

The determination of these nonsinusoidal waveforms will have a direct influence on computation of the conversion loss (or gain) and noise performance of microwave mixers, the stability and noise properties of parametric amplifiers, and the efficiency of harmonic generators. To an increasing extent, circuits are being designed using a multiple number of nonlinear elements (e.g., subharmonically pumped balanced mixers), and studies are being carried out using a device representation which includes several nonlinear elements (e.g., junction resistance and capacitance in a Schottky-barrier diode, series resistance and junction capacitance in an expitaxial varactor). When the nonlinear element is embedded in a circuit containing a small number of lumped linear elements, the nonsinusoidal waveforms can be determined by a time-domain integration of the network equations, carried over a sufficient number of cycles to allow steady-state conditions to be attained. However, this approach is impractical for most realistic microwave circuits, where the equivalent circuit of the linear network may well contain a large number (e.g., hundreds) of lumped and distributed elements. For this reason, in recent years, other numerical approaches have been developed for the accurate study of the excitation of nonlinear microwave circuits. These methods divide broadly into two categories: time-domain solutions, and the harmonic balance approach.

Time-domain solutions were initiated by Fleri and Cohen [1] who studied pumped resistive mixer diode waveforms. Their analysis, while it indicates the voltage waveform is far from sinusoidal, is highly simplified. In particular, the pump-source equivalent circuit is taken as resistive, and the complexities of diode packaging are largely ignored. The generality of this approach was improved through the work of Gwarek [2] who was able to replace an arbitrary embedding network by a single lumped-element network in series with a set of appropriately phased, harmonically related voltage sources; convergence problems, however, occur with this approach.

Harmonic balance approaches combine a Fourier analysis for the linear embedding network with a time-domain approach for the nonlinearity. An iterative procedure is then devised which balances (or equalizes) the harmonics in both the nonlinear and linear circuits. With the assumption of linear junction capacitance, Egami [3] analyzed a pumped mixer diode but found the convergence properties deteriorated significantly when more than two or three harmonics were considered. Gupta and Lomax [4] attacked the diode pumping problem by employing a variation of the harmonic balance approach in which voltage waveform estimates are updated until a stationary solution is reached; convergence problems appeared and remained unsolved. Kerr [5], [6] has achieved convergence for a wide range of circuits using the multiple reflection method, which requires insertion of a transmission line between the nonlinear and linear sections of the circuit. However, the complexity of the Kerr calculations together with the desire for deeper understanding of the convergence process, motivate further investigation. Hicks and Khan [7] have studied the problem by introducing a set of dual update algorithms together with a convergence parameter. Based on experience, satisfactory convergence rates are obtained by this method.

None of the above methods has yet provided a detailed convergence assessment to assist the user by providing prior information on the likelihood of convergence. It is clear that for the purposes of efficient automated nonlinear computation, the analysis algorithm and convergence mechanism should be thoroughly understood.

The purpose of this paper is to further develop and expand the method previously presented [7], in order to provide a detailed convergence assessment which will assist the user by providing prior information on the likelihood of convergence. The insight gained by this means is prerequisite to efficient automated computation of nonlinear microwave circuit behavior.

II. Numerical Analysis Methods

A. Voltage Update Method

The method described here is applicable to the analysis of the general circuit shown in Fig. 1, where a network containing linear and nonlinear elements is excited by a sinusoidal source $E(t)$. As shown in Fig. 1, the circuit is divided into two parts, one of which contains the nonlinear elements (as well as some linear elements for convenience) while the other part contains the remaining linear elements and the exciting source.

The analysis begins with selection of an estimated $V^N(t)$ value, designated $V_0^N(t)$; this value is usually taken at the exciting frequency, without harmonics, and may be found by an approximate calculation. Using $V_0^N(t)$, the corresponding periodic current $I_0^N(t)$ is found by a fourth-order Runge–Kutta method, unless there is a suitable analytical

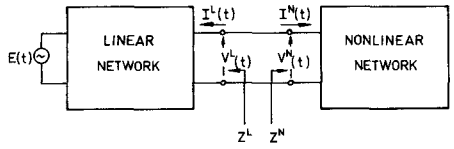

Fig. 1. Division of the general microwave circuit containing nonlinear elements.

expression available. Typically, 128 points are considered in the computation, allowing consideration of harmonics in $I_0^N(t)$ up to the sixteenth order with minimal truncation error in the Runge–Kutta integration.

Putting $I_0^L(t) = -I_0^N(t)$, we can use the fast Fourier transform to obtain $I_0^L(\omega)$, which is applied to the linear network. $V_0^L(\omega)$ is found by superposition, having components due to $I_0^L(\omega)$ and to the applied $E(t)$; the calculation is quite straightforward, since the network is linear.

Using an inverse fast Fourier transform we form $V_0^L(t)$ and compare it with the initial $V_0^N(t)$. If the difference is significant, the iteration proceeds with a new estimate of $V^N(t)$, designated by $V_1^N(t)$, and continues until the difference is sufficiently slight. The iteration procedure is a stationary one and therefore $V_1^N(t) = V_0^L(t) = V_0^N(t)$ at solution.

It remains now to specify how the new estimate is determined at the beginning of each successive iteration. At the kth iteration, consider a general

$$V_k^N(t) = \sum_{n=-M}^{M} V_{kn}^N e^{jn\omega t}$$

(where M has been set by the Runge–Kutta calculation) and the corresponding

$$V_k^L(t) = \sum_{n=-M}^{M} V_{kn}^L e^{jn\omega t}$$

which is determined by the process described above. The next iteration is carried out with a $V_{k+1}^N(t)$ having components

$$V_{(k+1)n}^N = p_n V_{kn}^L + (1-p_n) V_{kn}^N$$

where the p_n values are determined by convergence considerations, discussed below, and $0 < p_n \leq 1$. The use of a set of p_n values, described here as "convergence parameters", is a distinguishing feature of the method presented here and is an essential feature in ensuring convergence to the required solution.

1) Convergence: Let the true value of the voltage $V^N(t)$ be

$$V^T(t) = \sum_{n=-M}^{M} V_n^T e^{jn\omega t}.$$

Then $V_{kn}^N = V_n^T + \epsilon_{kn}$ where ϵ_{kn} is the error term. Likewise $V_{(k+1)n}^N = V_n^T + \epsilon_{(k+1)n}$ after one additional iteration.

$V^T(t)$, by definition, must satisfy the circuit constraints and thus

$$V_n^T = V_n^S - \frac{Z_n^L}{Z_n^N} V_n^T$$

where

V_n^S contribution due to the source voltage,
Z_n^L impedance presented by the linear network at the nth harmonic frequency in the absence of any source, and
Z_n^N impedance presented by the nonlinear network at the nth harmonic frequency as shown in Fig. 1.

Clearly, the value of Z_n^N will vary during the iteration process by virtue of the nonlinearity. With each iteration, Z_n^N changes until, in the case of the harmonics free from source voltages, it reaches $-Z_n^L$ at the solution. For the purpose of the convergence analysis, it will be assumed that the iterations are close to the solution and thereby Z_n^N changes only slightly. This strategy may be justified in two ways. Firstly, an iteration close to the solution should not diverge. Secondly, for iterations far from the solution, a convergence region (discussed below) sufficiently large to cover any variations in the Z_n^N may be obtained by appropriately setting the convergence parameter p_n. Now

$$\begin{aligned} V_{kn}^L &= V_n^S - \frac{Z_n^L}{Z_n^N} V_{kn}^N \\ &= V_n^S - \frac{Z_n^L}{Z_n^N}\left(V_n^T + \epsilon_{kn}\right) \\ &= -\frac{Z_n^L}{Z_n^N}\epsilon_{kn} + V_n^T \end{aligned}$$

using $V_n^T = V_n^S - \frac{Z_n^L}{Z_n^N} V_n^T$

$$\therefore V_{(k+1)n}^N = p_n\left(-\frac{Z_n^L}{Z_n^N}\epsilon_{kn} + V_n^T\right) + (1-p_n)\left(V_n^T + \epsilon_{kn}\right)$$

which yields directly, by substituting for $V_{(k+1)n}^N$, $\epsilon_{(k+1)n} = M_n^V \epsilon_{kn}$ where M_n^V is the error magnification factor for the nth harmonic component with the voltage update method, and is given by

$$M_n^V = 1 + p_n\left(-1 - \frac{Z_n^L}{Z_n^N}\right).$$

It is evident that we require $|M_n^V| < 1$ for all harmonics of interest to assure convergence of the iterative process. The speed with which convergence is obtained will also increase as the value of $|M_n^V|$ is decreased.

Note that the set of Z_n^N values will vary during the iteration process, because of the nonlinearity of the circuit elements. Hence any estimate of Z_n^N for convergence determination should be made on a "worst case" basis.

Insight into the choice of p_n for convergence may be obtained by plotting a set of curves of $|M_n^V| = 1$ on an impedance ratio plane defined by $W_n = Z_n^L / Z_n^N$ as shown in Fig. 2. The curves are a set of circles with center

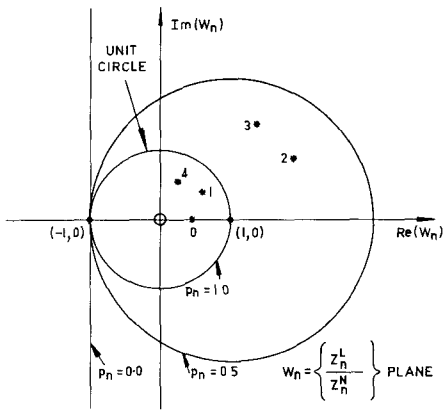

Fig. 2. Expansion of the voltage update convergence region due to changes in the convergence parameter p_n. The symbols (*) indicate a possible distribution of the first five harmonic impedance ratios (conjugates not shown).

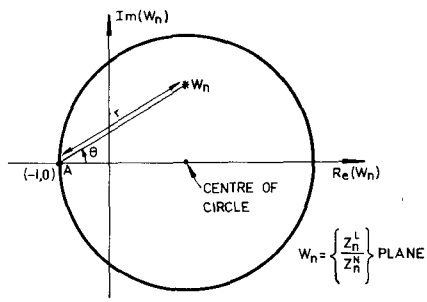

Fig. 3. Optimum real p_n for minimum M_n is given by $\cos\theta/r$, where θ is the angle between the line W_nA and the real axis; r is the length of W_nA.

$(-1+(1/p_n),0)$ and radius $1/p_n$, proceeding to the half-plane $\mathrm{Re}(W_n) \geq -1$ in the limiting case of $p_n \to 0$.

Using this diagram, the required p_n values for convergence are readily found, plotting W_n values for the harmonics of interest, and selecting a p_n set so that each W_n point lies within the p_n circle. In practice, it is usually possible to select a convergence parameter p which is used for all values of n. It is also possible to change the value of p as the calculation proceeds, and Z_n^N more closely approaches its true value; the purpose of this change is to make the values of the $|M_n^V|$ set as small as possible.

B. Current Update Method

There are many instances where the form of the nonlinear device characteristics is such that it is preferable to use current $I^N(t)$ as the independent variable rather than voltage $V^N(t)$. The resulting current update approach proceeds as the dual of the voltage update method, and is hence not described in detail.

It gives rise to an error magnification factor M_n^I defined by

$$\epsilon_{(k+1)n} = M_n^I \epsilon_{kn}$$

with the value of M_n^I determined by an approach similar to that used for M_n^V.

We find

$$M_n^I = 1 + p_n\left(-1 - \frac{Z_n^N}{Z_n^L}\right).$$

Hence we can plot a set of curves of $|M_n^I| = 1$ on an impedance ratio plane defined by $Z_n^N/Z_n^L = 1/W_n$. The curves on the $1/W_n$ plane are similar to those shown in Fig. 2 on the W_n plane, and the selection of the p_n set values proceeds in a similar manner to that for the voltage update method. Note that if W_n lies outside the circle of convergence for a specified p_n, with the voltage update approach, it will lie within the convergence circle for the same p_n value if the current update method is used.

C. Selection of the Convergence Parameters p_n

In both update methods, there is an optimum real p_n which minimizes the magnitude of each M_n. By simple calculation, this p_n is given by $\cos\theta/r$, where θ and r are defined in Fig. 3. However, the methods may be further extended by permitting p_n to become complex. This introduces the ability to perform phase rotations in the W_n plane. With this modification, given any W_n, M_n may in principle be set to zero. However, it should be noted that the error will not be zero following this iteration as the nonlinearity will present a different Z_n^N at the new operating point. Thus, although the new error is nonzero, it is considerably reduced.

It is clear the calculations of Z_n^N are necessarily approximate by virtue of the nonlinearity. Thus, as the iterations proceed, the W_n points will move across the plane. In the case of harmonics above the fundamental, the W_n points will all move towards the solution point $(-1,0)$, a condition which may be verified by Kirchoff's circuit laws.

For most practical situations, the following guidelines will ensure convergence. An examination of the linear circuit impedances at the high harmonics will determine which of the update methods should be used, i.e., large linear circuit impedances above the fundamental require the current update approach. Having selected the appropriate update approach, each complex p_n can be calculated such that M_n is set to zero. However, tests have shown that the advantages of using complex p_n over real p_n are slight, resulting in only marginal improvements in efficiency in practical situations. Moreover, rather than use the optimal real p_n given in Fig. 3, a value of p, which is valid for all n, may be used. Although this situation is clearly not optimal, this simplification has been found to produce relatively efficient convergent conditions in most practical situations encountered.

III. Identity Networks

Modifications of the basic harmonic balance approach are possible by introducing a special class of networks at the nonlinear–linear circuit interface (Fig. 4). The purpose of these networks is to preserve the overall circuit performance while altering the harmonic impedance ratios to

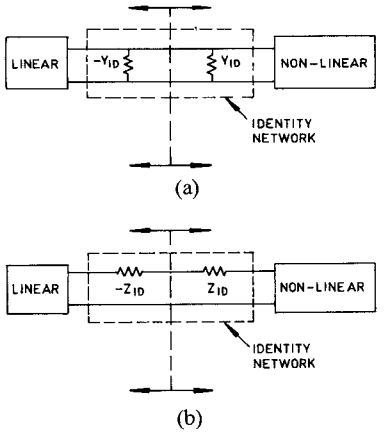

Fig. 4. Identity networks: (a) voltage update identity element; (b) current update identity element.

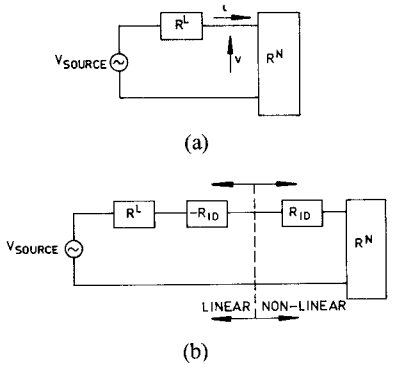

Fig. 5. Application of an identity element: (a) pumping circuit with a current modulated nonlinear resistance: $R^N = 10(1+I)\ \Omega$, $R^L = 1\ \Omega$, $V_{source} = \cos(\omega t)$; (b) addition of the current update identity element.

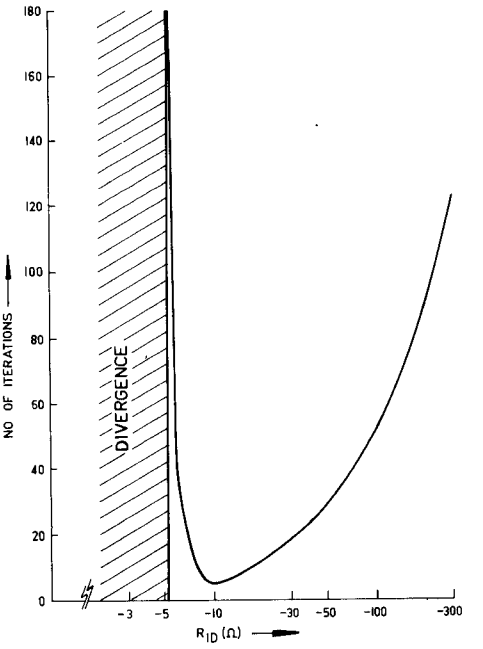

Fig. 6. Convergence rate versus the identity element value. Convergence was deemed to have occurred when the error became less than 0.1 percent.

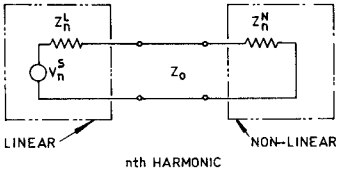

Fig. 7. Distributed identity element.

improve the convergence rate. The term "identity network" is introduced to describe networks which satisfy this property. Identity networks may be subdivided into two classes, viz, lumped and distributed.

A. Lumped Identity Networks

Two examples of lumped identity networks are shown in Fig. 4. To utilize them, these networks are bisected with one of the identity elements assigned to the linear one-port and the matching identity element included in the nonlinear network. For ease of nonlinear circuit computation, the network depicted in Fig. 4(a) is suitable for voltage update solutions while that of Fig. 4(b) is more convenient to use with current update solutions. These networks maintain the overall circuit performance but alter the harmonic impedance ratios and thereby the convergence rates.

The following example illustrates the use of a current update lumped identity element. A nonlinear element is fed from a simple resistive voltage source shown in Fig. 5(a). The resistance of the nonlinear element consists of a fixed 10 Ω together with a current modulated value of $10I$ Ω, where I is in amps.

It would be advantageous to use a current update approach so that the nonlinearity could be handled without resorting to the use of quadratic equations. Without modification, the circuit requires a voltage update approach as the harmonic impedance ratio R^L/R^N is approximately 0.1 for all harmonics. However, the problem may be transformed to a current update problem with an identity negative resistance of the order of $-10\ \Omega$ as shown in Fig. 5(b).

The circuit was analyzed as described and Fig. 6 depicts the dependence of the current update convergence rate on the identity element value. For small values of R_{ID}, the circuit problem is a voltage update candidate and therefore the solution diverges on using the current update algorithm. Larger values of R_{ID}, however, ensure current update convergence with an optimum value of R_{ID} being approximately $-10\ \Omega$.

B. Distributed Identity Elements

Distributed identity elements may also be used in a similar way to their lumped counterparts. The Kerr [5] multiple reflection method of circuit analysis may be regarded as an update harmonic balance method in which use of these distributed elements is exploited. A lossless transmission line is inserted in cascade at the circuit interface (Fig. 7), its electrical length being set at an integral number of pump wavelengths to preserve the steady-state

solution. The presence of a distributed element requires that both the voltages and currents be updated simultaneously in the iteration process. Kerr [5] details the algorithm necessary to compute the voltages, currents, and propagating waves. By suitably rearranging Kerr's equations, it can be shown that successive voltage and current iterates are given by

$$V^N_{(k+1)n} = \rho^L_n \rho^N_n V^N_{kn} + \frac{Z_0}{Z_0 + Z^L_n} V^S_n$$

$$I^N_{(k+1)n} = \rho^L_n \rho^N_n I^N_{kn} + \frac{Z_0}{(Z_0 + Z^L_n)(Z_0 + Z^N_n)} V^S_n.$$

The reflection coefficients are defined in the usual way, viz.,

$$\rho^N_n = \frac{Z^N_n - Z_0}{Z^N_n + Z_0}$$

$$\rho^L_n = \frac{Z^L_0 - Z_0}{Z^L_n + Z_0}$$

where Z_0 is the characteristic impedance of the transmission line. Clearly, the successive errors as convergence is approached are given by

$$\epsilon_{(k+1)n} = \rho^L_n \rho^N_n \epsilon_{kn}$$

and thus convergence is assured if the products $\rho^L_n \rho^N_n$ fall within the unit circle. This condition applies for most stable systems and thus the Kerr method has been reported to have satisfactory convergence properties [6]. Since Z_0 is arbitrary, the convergence process can be optimized by adjusting its value; from estimates of the range of values taken by Z^N_n during the iteration process, Z_0 would be chosen such that the maximum value of the products $|\rho^L_n \rho^N_n|$ is minimized.

The parameter p_n used in the basic update approaches may also be introduced into the multiple reflection approach. The error magnification coefficient with the addition of the parameter p_n is then given by

$$M^K_n = 1 + p_n(\rho^L_n \rho^N_n - 1)$$

and variations in p_n once again provide expanded circular areas of convergence.

It should be noted that all the modifications to the update algorithms discussed in this paper can be used simultaneously, i.e., distributed elements may be added to lumped identity networks and so on. However, as the examples in Section V illustrate, most circuits can be analyzed using only the basic voltage and current update algorithms.

IV. Comparison With Other Methods

Only two methods in the literature satisfy the requirement of convergence under general conditions, namely Kerr's [5] multiple reflection method and the update approaches described here. A convergence comparison for a particular example has been previously reported [7] between these two methods. More generally, the convergence rates of the update approach may be expected to be superior to that of the multiple reflection approach. Typically, the impedance of microwave circuits will approach either open or short-circuit conditions with increasing frequency. Such conditions enhance the performance of the two update methods whose convergence rates are a direct function of the proximity of the impedance ratios to the origin, i.e., the proximity of the linear impedances to open and short circuit conditions. In direct contrast, the multiple reflection approach performs optimally under conditions of match at high frequency; such conditions are unlikely to be found in practice irrespective of the choice of the impedance parameter Z_0.

V. Examples

Three examples are given here to demonstrate the generality and flexibility of the voltage and current update algorithms. An example illustrating the voltage update method has already been reported [7]. The examples given here report numerical analyses of the pumping of various solid-state diodes, each of which is post mounted in waveguide conditions as shown in Fig. 8. The equivalent circuit of Eisenhart and Khan [8] is used in each case to determine the embedding impedances seen at the post mount terminals. A simple pi-circuit satisfactorily accounts for the effects of packaging in each diode (Fig. 9).

A. Varactor Diode Pumping Circuit

This example illustrates the nonlinear analysis of the pumping of a varactor diode in the *X*-band waveguide circuit given above (Fig. 8) for use in the accurate prediction of parametric amplifier performance. An accurate calculation of the harmonic components of the elastance waveform is essential for successful investigation of parametric amplification where small circuit changes in the harmonic terminating impedances can lead to substantial changes in operating performance. Matching of the diode to the waveguide was achieved using a variable short circuit and the variable inductive iris placed at a fixed distance from the post plane. An ideal filter presenting a short circuit at all harmonics of the fundamental pump frequency was used to confine power losses at the harmonic frequencies to the diode series resistance. The packaging and diode details are given in the caption to Fig. 10.

The strategy employed in the computer analysis of the above circuit can be divided into three major steps:

1) the conditions required to match the nonlinear diode to the waveguide at the pump frequency of 10 GHz were determined;
2) equivalent circuits, valid at the diode terminals looking outwards into the waveguide, are determined for the fundamental and its harmonic frequencies;
3) the results of step 2) are combined with the diode capacitance characteristic, and fed into the nonlinear circuit analysis program described above.

Due to the large waveguide impedances present in the linear circuit, a current update solution was necessary for convergence. All p_n were set to unity and convergence was

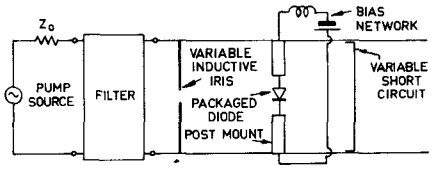

Fig. 8. Waveguide mount circuit used for the three solid-state diodes analyzed here.

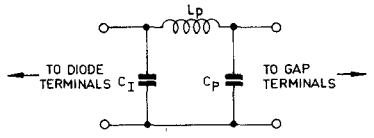

Fig. 9. Equivalent circuit to represent the effects of diode packaging.

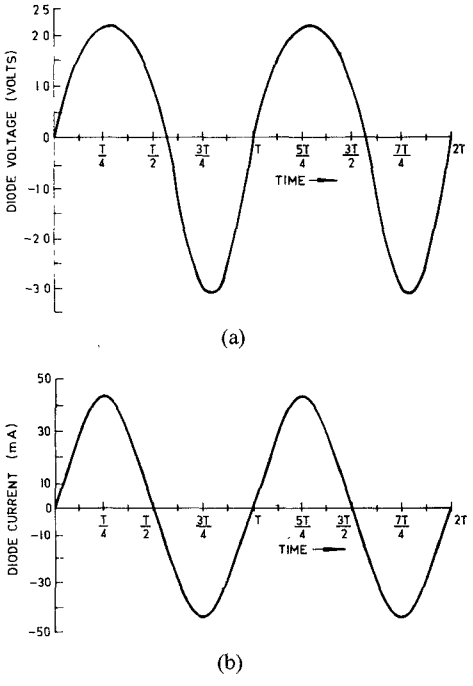

Fig. 10. Varactor diode junction waveforms: (a) terminal voltage; (b) terminal current. The parameters of the varactor diode analyzed were $R_S = 4.0\ \Omega$, $C_0 = 0.5$ pF, $\phi = 0.6$ V, $\gamma = 0.5$. The package parameters were $C_p = 0.2$ pF, $C_t = 0.05$ pF, $L_p = 0.9$ nH. The bias voltage used was -2.0 V.

achieved in 30 iterations. Following Kerr [5], convergence was deemed to have occurred when the harmonic impedance ratios were within 0.5 percent of unity. To obtain the varactor junction voltage from the known diode current (i.e., $V^N(t)$ from $I^N(t)$), a nonlinear integration of the varactor equation was performed using the classical Runge–Kutta algorithm. Only one iteration was required here since the integration constant may be determined from dc bias constraints.

Fig. 10 shows typical varactor diode current and voltage waveforms. The almost sinusoidal diode current reflects the relatively large waveguide impedances at the pump harmonic frequencies. The elastance waveform may be Fourier analyzed as follows:

$$S(t) = \sum_{n=-\infty}^{\infty} S_n e^{jn\omega t}.$$

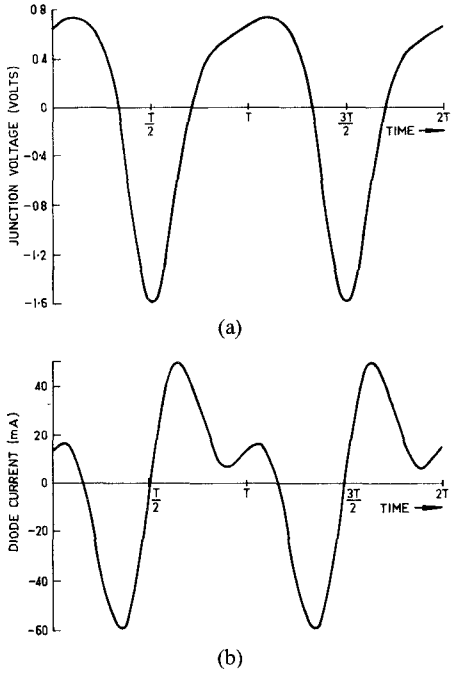

Fig. 11. Mixer diode junction waveforms: (a) terminal voltage; (b) terminal current. The parameters of the mixer diode analyzed were $I_{sat} = 8\times10^{-15}$ A, $(q/\eta kT) = 39\ V^{-1}$, $R_s = 1.27\ \Omega$, $C_0 = 0.1$ pF, $\phi = 0.85$ V, $\gamma = 0.5$. The package parameters were $C_p = 0.02$ pF, $C_t = .002$ pF, $L_p = 0.08$ nH.

TABLE I
HARMONIC ELASTANCE VALUES
(REFERRED TO DC ELASTANCE VALUE)

n	$\lvert S_n/S_0 \rvert$
1	0.33
2	3.0×10^{-3}
3	3.0×10^{-5}

The harmonic elastance coefficients for the waveforms shown in Fig. 10 are given in Table I. An extensive analysis [10] of the above varactor diode pumping situation has shown the values in Table I are fairly typical unless the post geometry is such as to create resonant conditions at the pump frequency.

B. Schottky-Barrier Diode Mixer

Mixer waveform analyses are an important application of nonlinear analysis techniques. Held and Kerr [9] and Kerr [6] have completed comprehensive investigations of a variety of mixer circuits but have relied on an experimental determination of the embedding impedance. In this example, analytical determination of the mount impedance is carried out using the Eisenhart and Khan [8] equivalent circuit. This circuit was analyzed in a similar fashion to the varactor circuit. For simplicity, the matching network elements, namely the ideal filter and the iris in Fig. 8 are removed. The diode waveforms were numerically analyzed for conditions of 60-GHz excitation in a 50–75-GHz standard waveguide. The diode parameters, given in the caption to Fig. 11, are for a typical Schottky-barrier diode used in millimeter-wave mixers [11].

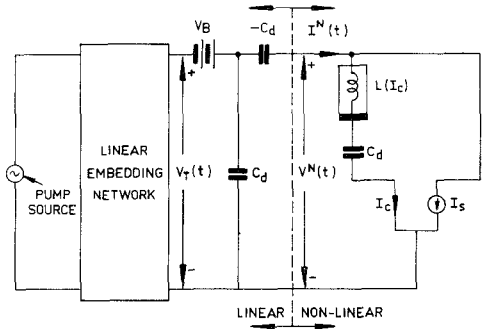

Fig. 12. IMPATT diode equivalent circuit used in the analysis showing the connection to the embedding network and the position of the linear–nonlinear circuit interface.

TABLE II
CALCULATED MIXER CONVERSION VALUES

n	$G_n\Omega^{-1}$	$C_n \times 10^{-13}$ F
0	0.0808	1.4155
1	0.1839+j.6721	0.4247−j.1364
2	0.567−j.5452	−0.246−j.1077
3	−.0195+j.0522	−.0504−j.0396

As before, the current update method was used due to the large harmonic impedances presented by the linear waveguide circuit. Fig. 11 shows the diode current and junction voltage waveforms obtained from the nonlinear analysis program. 150 iterations were required for convergence using 0.75 for all p_n. As in the varactor diode example, convergence was deemed to have occurred when the harmonic impedance ratios were within 0.5 percent of unity. To derive $V^N(t)$ each time from the current $I^N(t)$ required a nonlinear integration due to the time-varying capacitance. Due to the forward voltage saturation in the exponential diode, generally only three iterations were required to obtain a periodic solution. The Fourier conductance and capacitance waveform coefficients necessary to compute the mixer admittance matrix [6], [9] are given in Table II.

The nonlinear analysis update methods have been extended to the case of more than one nonlinearity. This theory has been used to study subharmonic mixer circuits, the results of which have been reported [12], [13].

C. *Negative Resistance* IMPATT Mixer

A numerical pump analysis technique of this type is essential for investigation of IMPATT negative resistance mixers. The nonlinear voltage–current relation in the IMPATT diode can be analyzed using the voltage update method, together with the IMPATT model developed by Gupta [14] from the Read equations (Fig. 12). The Gupta model, although valid for arbitrary waveforms, does not model the effect of the back bias effect explained by Brackett [15]. Furthermore, although Gupta states the parameter V_B does not enter into the RF performance directly, it may be shown [16] that V_B depends on both frequency and the RF signal level and thus is not constant.

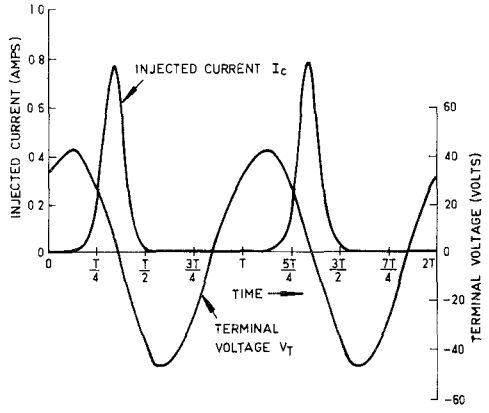

Fig. 13. Variation of the injected current I_c and the IMPATT terminal voltage V_T with time. The parameters of the IMPATT diode analyzed were: $I_{dc} = 100$ mA, $\tau_d = 35$ ps, $L_a = 1.4$ nH, $C_d = 0.35$ pF. The package parameters were $C_p = 0.20$ pF, $C_i = 0.05$ pF, $L_p = 0.90$ nH.

However, it is a useful starting point for an IMPATT waveform analysis.

The nonlinear inductor and current source in the model are defined by

$$L(I_c) = \left(\frac{I_{dc}}{I_c}\right) L_a$$

$$I_s(t) = \frac{1}{\tau_d}\int_{t-\tau_d}^{t} I_c(t')dt' - I_c(t)$$

where

I_c injected current in the IMPATT diode,
I_{dc} dc IMPATT diode current,
I_s "memory" current source in the IMPATT model,
τ_d transit time for the drift region in the IMPATT diode, and
L_a IMPATT avalanche inductance.

As with the preceding examples, the linear equivalent circuit includes the effects of both packaging and the waveguide post mount. As with the Schottky-barrier diode mixer, the matching elements are ignored. Pumping at 8 GHz in an X-band waveguide was studied using the typical IMPATT diode parameters [14] shown in the caption to Fig. 13.

The nonlinear circuit is composed of only a portion of the IMPATT model. As Fig. 12 shows, the two depletion capacitances are assigned to the linear circuit. Due to the shorting action of these two capacitances, the linear impedances are small at high frequencies and the voltage update approach was therefore successful. Convergence was obtained in 7 iterations with all p_n values being unity, the convergence criterion being the requirement that the harmonic impedance ratios were within 0.5 percent of unity. Obtaining the nonlinear current $I^N(t)$, given the IMPATT voltage $V^N(t)$, requires an inversion of the above differential equation using the Runge–Kutta method. Such an operation required only one iteration, the dc bias constraints determining the value of the integration constant. Typical waveforms at 8 GHz are shown in Fig. 13, the

IMPATT impedance at the fundamental frequency being $-11.0-j65.9\ \Omega$.

VI. Conclusions

This paper has investigated the factors affecting the convergence of the voltage and current update approaches previously reported [7]. With the aid of the convergence formulas developed in this paper, a suitable iteration technique may be chosen prior to the execution of the computer program. The effect of the convergence parameter has been illustrated graphically on a convergence diagram. The multiple reflection technique of Kerr [5] has been shown to be a special case of the more general technique described in this paper; its convergence properties are shown to be dependent on the transmission line impedance, enabling an optimum value to be chosen. Three solid-state diode pumping examples, together with a theoretical example, show the potential of the voltage update and current update approaches in numerical pumping analysis.

References

[1] D. A. Fleri and L. D. Cohen, "Nonlinear analysis of the Schottky-barrier mixer diode," *IEEE Trans. Microwave Theory Tech.*, vol. MTT-21, pp. 39–43, Jan. 1973.

[2] W. K. Gwarek, "Nonlinear analysis of microwave mixers," M.S. thesis, Massachusetts Inst. Tech., Cambridge, MA, Sept. 1974.

[3] S. Egami, "Nonlinear, linear analysis, and computer-aided design of resistive mixer," *IEEE Trans. Microwave Theory Tech.*, vol. MTT-22, pp. 270–275, Mar. 1974.

[4] M. Gupta and R. Lomax, "A self-consistent large signal analysis of a Read-type IMPATT diode oscillator," *IEEE Trans. Electron Devices*, vol. ED-18, pp. 544–550, Aug. 1971.

[5] A. R. Kerr, "A technique for determining the local oscillator waveforms in a microwave mixer," *IEEE Trans. Microwave Theory Tech.*, vol. MTT-23, pp. 828–831, Oct. 1975.

[6] A. R. Kerr, "Noise and loss in balanced and subharmonically pumped mixers: Parts I and II: Theory and application," *IEEE Trans. Microwave Theory Tech.*, vol. MTT-27, pp. 938–950, Dec. 1979.

[7] R. G. Hicks and P. J. Khan, "Numerical technique for determining pumped nonlinear device waveforms," *Electron. Lett.*, vol. 16, no. 10, pp. 375–376, May 1980.

[8] R. L. Eisenhart and P. J. Khan, "Theoretical and experimental analysis of a waveguide mounting structure," *IEEE Trans. Microwave Theory Tech.*, vol. MTT-19, pp. 706–719, Aug. 1971.

[9] D. N. Held and A. R. Kerr, "Conversion loss and noise of microwave and millimeter-wave mixers: Parts 1 and 2: Theory and experiment," *IEEE Trans. Microwave Theory Tech.*, vol. MTT-26, pp. 49–61, Feb. 1978.

[10] R. G. Hicks, P. J. O'Shea, and P. J. Khan, "Computer-aided nonlinear analysis of varactor diode pumping in waveguide circuits," in *Proc. IREECON*, (Sydney, Australia), Aug. 1979, pp. 391–394.

[11] J. A. Calviello, "Advanced devices and components for the millimeter and submillimeter systems," *IEEE Trans. Electron Devices*, vol. ED-26, pp. 1273–1281, Sept. 1979.

[12] R. G. Hicks and P. J. Khan, "Analysis of balanced subharmonically pumped mixers with unsymmetrical diodes," in *Proc.* 1981 *IEEE/MTT-S Int. Microwave Symp.*, (Los Angeles), June 1981, pp. 457–459.

[13] R. G. Hicks and P. J. Khan, "Nonlinear–linear analysis of subharmonic mixers with dissimilar diodes," in *Proc. 1981 IREE Int. Conf.*, (Melbourne), Aug. 1981, pp. 100–102.

[14] M. S. Gupta, "A nonlinear equivalent circuit for IMPATT diodes," *Solid-State Electron.*, vol. 19, pp. 23–26, Jan. 1976.

[15] C. A. Brackett, "The elimination of tuning-induced burnout and bias-circuit oscillators in IMPATT oscillators," *Bell Syst. Tech. J.*, vol. 52, Mar. 1973, pp. 271–306.

[16] B. D. Bates, private communication.

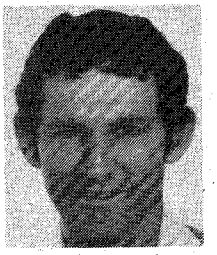

Ross G. Hicks (S'76) was born in Southport, Australia on February 27, 1956. He received the B.E. (Communications, with First Class Honours) degree from the University of Queensland, Brisbane, Australia, in 1976, and has since then been investigating resistive mixers as the basis of the Ph.D. degree.

His research interests also include computer circuit analysis methods, waveguide equivalent circuits, and microwave solid-state circuit design.

Mr. Hicks is a member of the Institution of Radio and Electronics Engineers, Australia and the Institution of Engineers, Australia.

Peter J. Khan (M'61–SM'79) was born in Bowral, Australia on November 12, 1936. He received the B.Sc. degree in mathematics and physics, and the B.E. and Ph.D. degrees in electrical engineering, all from the University of Sydney, Australia in 1957, 1959, and 1963 respectively.

From 1953 to 1959 he was employed at the Weapons Research Establishment at Salisbury, South Australia, carrying out research and development in electronic circuits. After completion of his doctoral studies in parametric amplification, he came to the University of Michigan in Ann Arbor, MI, in 1963 with a Fulbright Postdoctoral Fellowship. He remained there until 1976, as Assistant Professor and Associate Professor of Electrical Engineering. In 1976 he returned to Australia where he is now Reader in Electrical Engineering at the University of Queensland. His research interests include microwave solid-state circuit design, as well as fabrication and analysis of propagating structures at millimeter-wave and optical frequencies.